



## Electrical Impedance Tomography Signal Conditioning for Lung Imaging Applications

**Nur Amira Zulkifli<sup>1</sup>, Kaviarasu Nandaguru<sup>1</sup>, Omar Fahmi Arm<sup>1</sup>, Feisal Mohamed Khamis<sup>1</sup>, Ahmad Ridhwan Bin Wahap<sup>2</sup>, Fatin Aliah Phang Abdullah<sup>3,4</sup>, Tee Kian Sek<sup>5</sup>, Nurul Hidayat<sup>6</sup>, Jaysuman Pusppanathan<sup>1,7,\*</sup>**

<sup>1</sup>Department of Biomedical Engineering & Health Sciences, Faculty of Electrical Engineering, Universiti Teknologi Malaysia, 81310 Skudai Johor, Malaysia

<sup>2</sup>Faculty of Electrical Engineering, Universiti Teknologi Malaysia, 81310 Skudai Johor, Malaysia

<sup>3</sup>Centre of Engineering Education, Universiti Teknologi Malaysia, 81310 Skudai Johor, Malaysia

<sup>4</sup>School of Education, Faculty of Social Sciences and Humanities, Universiti Teknologi Malaysia, 81310 Skudai Johor, Malaysia

<sup>5</sup>Jabatan Kejuruteraan Elektronik, Fakulti Kejuruteraan Elektrik dan Elektronik, Persiaran Tun Dr. Ismail, 86400 Parit Raja, Johor, Malaysia

<sup>6</sup>Department of Physics, Faculty of Mathematics and Natural Sciences, Universitas Negeri Malang, Jl. Semarang 5, Malang 65145, Indonesia

<sup>7</sup>Sports Innovation & Technology Centre (SITC), Institute of Human Centred Engineering (iHumEN), Universiti Teknologi Malaysia, 81310 Skudai Johor, Malaysia

\*Corresponding author [jaysuman@utm.my](mailto:jaysuman@utm.my)

Received 27 June 2023; Accepted 06 August 2023; Available online 06 August 2023  
<https://doi.org/10.11113/humentech.v2n2.58>

### Abstract:

Electrical impedance tomography (EIT) imaging is capable for human lung imaging based on its continuous self-monitoring capabilities, and suitability for daily routines. This paper introduces a simulation work for EIT signal conditioning circuit and its simulated waveform response using Multisim software. EIT circuit simulations consist of several signal processing circuits for the receiving part of the EIT, band pass filter circuit, amplifier, and analog-to-digital circuit. The system produced a unit function signal of 5V from an input 250 kHz sine function via band pass filter, operational amplifier and AC/DC conversion. The waveform pattern result is presented for each processing stage aim to demonstrate the basic work of an EIT circuitry setup.

Keywords: Electrical impedance tomography; Lung imaging; Biomedical; Circuit design; Band-pass filter

## 1. Introduction

Electrical impedance tomography (EIT) is one of the most popular lung imaging approaches due to the cost effective and high efficiency characteristics of the approach. In general, the electrical properties of different materials are distinct from each other, and these differences produce varied distribution of electrical impedance within a volume. The general principle of EIT is an inverse problem which determines the digital values of currents and voltages at the electrodes within the region of interest placed on the boundaries and the evaluation of impedance on the region provides the

necessary information for imaging. There are many reviews and technical studies regarding the principles and functionality of EIT devices and techniques in lung imaging. In fact, EIT can be characterized by the combination of electrical capacitance tomography (ECT) and electrical resistance tomography (ERT). The two main functional components of ECT and ERT devices are the capacitance (permittivity) and resistance (conductivity) respectively [1]. However, practitioners explain that EIT as an approach that uses conductance component. Among the existing EIT methods, the most challenging issue is the determination of the material distribution within the ill-posed boundary regions. In many cases, this problem not only produces one solution but also many reconstruction algorithms are needed to develop and implement for the numerical construction of the material distribution within the interest region [1–5]. Though, the image resolution and depth of the EIT systems are not as robust as other tomography techniques, yet these drawbacks can be potentially compensated cost effectiveness and safety standard of the EIT systems. There is also another type of EIT system, EITS, also known as Multi-frequency EIT. This EITS system is composed electrical impedance spectroscopy (EIS) and EIT systems and uses frequency dependent properties of materials in the frequency domains [5, 6].

One of the reasons that governs the practicality and applications of EITS systems and associated methods is the characteristics behaviors of the electrical impedance of different biological tissues. This distinct characteristic is very helpful in image-based monitoring and observation of the functions of various vital tissues and organs including a very cost effective and higher safety standard. Another crucial benefit of adapting EITS in clinical health care is the availability and portability of the EIT devices in isolated and remote areas as essential medical equipment where immediate hospital facilities and ambulance services are not accessed easily. Detection and imaging of breast cancer [3, 7–9], monitoring the air flow volume in the lungs [10], classification of the brain strokes [11, 12], detection of the skin cancer [13] and other applications of EIT systems were used in many studies. Moreover, detection of the material acceleration in the other fluidic mixtures, i.e., movement of the water particles in ice and water mixtures, could also be observed with the EITS systems, particularly if the systems are incorporated with other technologies [14]

In the application of mechanical ventilation imaging, EIT is a most favorable approach due to its real time, radiation free and non-invasive characteristics. Though conventional EIT systems could have a belt of either 16 electrodes or 32 electrodes, the electrode placement and functionality of both channel EIT are almost similar. In both EIT systems (16 and 32 channels), the electrodes are placed around the chest wall as well as a reference electrode which is placed in the central section of the body, usually abdomen, for the measurement of regional electrical bioimpedance. In the majority of cases, the transverse plane, often the place between the 4th and 5th intercostal space, is the placement region of the 16-channel electrode belt. However, due to the possibility of interaction of diaphragm with the measurement plane, it is often recommended that the 16-channel electrode belt be placed lower than the 6th intercostal region [15–18].

The principal technical process of EIT based observation or imaging involves applying low amplitude and high frequency alternating electric currents via a pair of electrodes and measuring the surface potentials by the other electrodes. The bioelectrical impedance can be established by applying the Ohm's law between the known applied current and measured voltage of the injection and measurement electrodes. Afterward, the adjacent electrode pair is used for the next current application, and the other 13 measurements of voltage are carried out. Therefore, according to this set up, a complete cycle of rotation is implemented by applied electric currents and voltage measurements by the adjacent pairs of electrodes, which in turn creates a 16 electrode positions while each of the position is encompassed by 13 voltage measurements [17]. Therefore, there are a total of 208 resulting values, also known as raw images. These raw images are then constructed together in order to produce the transverse EIT image. However, existing commercially available EIT devices could produce images of 50 frame per second (fps), which is considered a relatively high scanning rates of image.

## 2. Background Study

There are many effective and high-end imaging technologies, such as magnetic resonance imaging (MRI). Computed tomography (CT) scan and X-ray, for the functional monitoring of pulmonary functions. These existing imaging techniques provide highly resolute spatial images of lungs and other tissues and organs. Nevertheless, in case of CT-scanners and X-ray imaging, the patients are exposed to ionizing radiation and for repeated imaging this radiation could have detrimental effects to the patient's seeking ventilation and perfusion imaging [19]. Moreover, these devices are heavy, and therefore are kept at stationary facilities, and require a high capital of maintenance cost as well as imaging cost. EIT provides an alternative solution for these disadvantages in lung function monitoring [20, 21]. In surgery, the applications of EIT devices are very promising in case of many diseases for the detection and real-time imaging purposes of common and serious complications occurring during thoracic and pulmonary surgery [6, 14, 15, 20]. However, due to the cost effectiveness and portability of the EIT devices, patients' home monitoring and bed-side monitoring are more reliable for the real-time and continuous observation of pulmonary and thoracic functions [20, 22]. EIT systems and techniques are also very useful in monitoring the conditions of pre-mature birth since lung immaturity is the primary

cause of premature. Hence, monitoring and observation of the development of pre-term neonates’ lungs are easily performed by the ionizing radiation free EIT [23]. In another word, the advent and development of the EIT devices had made the image-based monitoring of lung’s functionalities over a wide range of patients including pre- and post-term neonates lung EIT techniques are developing at an astounding rate and this area is becoming a separate milestone for the clinical diagnosis and medical imaging [24–26].

During the clinical procedures and observation of patients with acute lung injury, positive pressure ventilation is a mandatory process of ensuring the exchange of the adequate volume of gas within the respiratory system. However, the adequate exchange of pulmonary gas within the respiratory systems is maintained by mechanical ventilation during the treatment of the underlying diseases [27]. Though, during the mechanical ventilation process, over distension could lead to severe lung injury if very high pressure is applied, for some specific patients, in order to obtain sufficient tidal volume within the respiratory systems. The damage or injury caused by mechanical ventilation is also known as ventilator induced lung injury (VILI). Therefore, researchers and professionals from various disciplines and sectors focus their studies on protective ventilation strategies in order to prevent VILI related complications and damage during mechanical ventilation [28–30]. Therefore, the development of the EIT devices is a potential step in order to prevent and minimize, in most cases, the VILI associated complications and damages during the mechanical ventilation. The proposed EIT system of this study could be further modified to improve the special resolution and efficiency of the real-time image-based monitoring of the lung activities during the mechanical ventilation process while treating the underlying disease of the patients with existing lung complications or injuries.

Generally, the mathematical concept of EIT is formulated by applying the simple Ohm’s Law equation:

$$E = I R \tag{1}$$

where an electric field (E), current (I) and a resistance (R) as shown in Equation 1. Rather than using simple resistance, instead conductivity will be used, and by expanding voltage into an electric potential and assuming no significant current is generated from the body, Equation (1) hence becomes:

$$J = \sigma E \tag{2}$$

where current density (J) and conductivity ( $\sigma$ ) is compared to Maxwell’s equation for electromagnetic wave transmission [2]:

$$\nabla \times E = - \partial B / \partial t, \text{ and } \nabla \times B = \mu_0 \epsilon_0 \partial B / \partial t \tag{3}$$

for a measured set of potentials there exist some set of conductivities ( $\sigma$ ). The set of potentials acquired by the EIT system act as the boundary conditions, allowing the conductivities to be solved. However, this is not a well-posed problem in that many solutions may exist that reflect the boundary conditions. The conductivities are non-linear as well, making the solution(s) more difficult to obtain.

### 3. Methodology

This virtual experiment study was carried out for circuit simulation work using Multisim software. The EIT circuit simulations consisted of several circuits as in Figure 1 breakdown, which are signal generating circuit, band pass filter circuit, amplifier, and analog-to-digital circuit. The circuit simulations were carried out in several phases of sine wave signal generation, adding white noise to the input signal, filtering the signal using pass band filter, amplifying the filtered signal and analog-to-digital conversion.

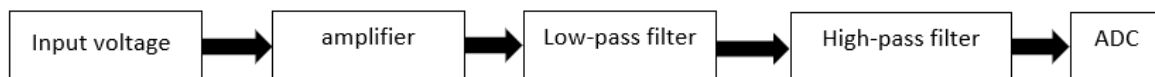


Figure 1 Flow diagram of the signal conditioning for EIT

#### 3.1 Circuit layout

The input of EIT consists of a power source along with alternating current (AC) sine wave which supplies voltage to the whole system. The simulation of the input is expressed by an AC voltage source paired with a potentiometer circuit

for the adjustment of the input amplitude, the simulated amplitude and frequency were generated similar to the generalized capacity of regular power sources. Figure 2 shows the generated input signal.

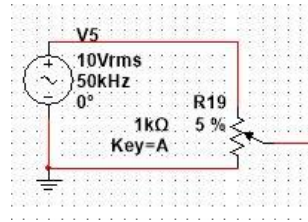


Figure 2 Input signal for receiver electrode (RX)

In real practice, noises are inevitable and therefore a white noise is applied to the input signal (Figure 3). White noise is a random signal having equal intensity at different frequencies, giving it a constant power spectral density. For that, the white noise signal has been added so that the filter can be tested and verified, Figure 3 shows the white noise signal circuit.

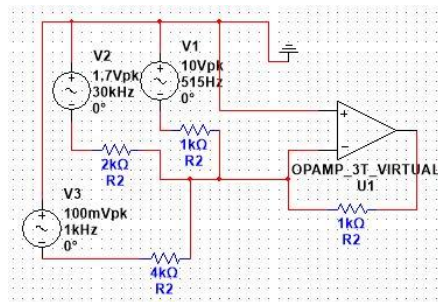


Figure 3 White noise signal circuit

One of the most important elements of the EIT input is the filter circuit. The simulated filter circuit was designed to accommodate the range of voltage and frequency that the EIT requires for a tomography. The filter circuit designed was band pass filter which passes frequencies within a certain range and rejects (attenuates) frequencies outside that range, the range of EIT operational frequency is between 10 to 250 kHz. This range of low frequency is within kilohertz which is suitable for further image reconstruction and filtering circuit to avoid saturated signals. Figure 4 shows the band pass filter which is the combination of low pass and high pass filter for noise filtering.

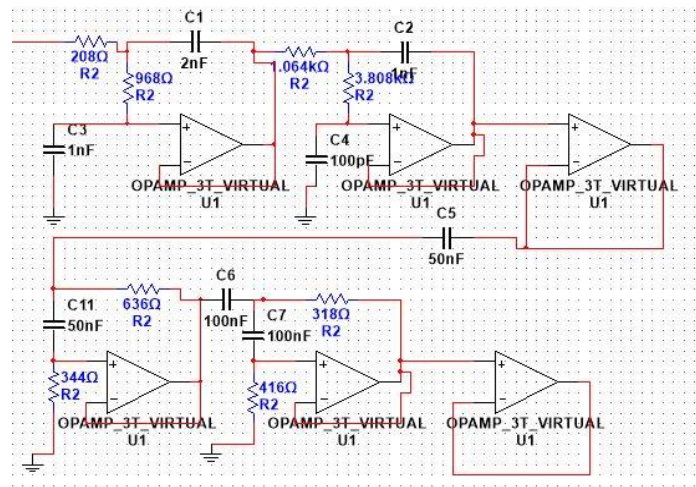


Figure 4 Band pass filter

Operational amplifier is the next phase after filtering the input signal. An operational amplifier is an integrated circuit that can amplify weak electric signals that is used to amplify the amplitude of the signal after it is being filtered, which lowers the value of the amplitude. An operational amplifier has two input pins and one output pin. Figure 5 shows the operational amplifier.

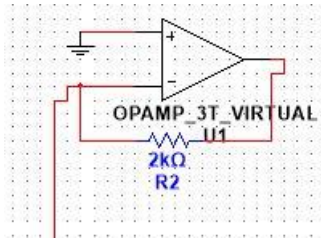


Figure 5 Operational amplifier

The end step for the circuit is analog-to-digital conversion. Analog-to-digital converter is an electronic integrated circuit used to convert the analog signals such as voltages to digital or binary form consisting of 1s and 0s. Most of the ADCs take a voltage input as 0 to 10 V, -5 V to +5 V, and correspondingly produce digital output as a binary number, Figure 6 shows the analog-to-digital converter.

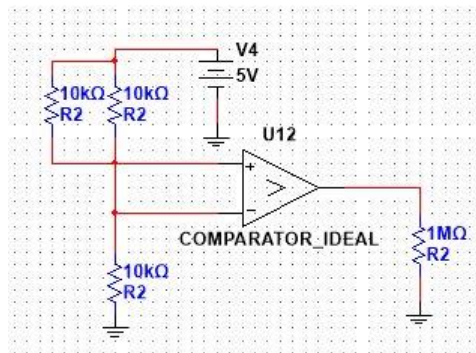


Figure 6 Analog-to-digital convertor

#### 4. Result

Each element of the circuit built and simulated presents its unique output, only their summation after each other exhibits the output of the EIT. The first output is from the input AC circuit which ranged from -13 V to +13 V and is shown in Figure 7, in addition Figure 8 shows the output of the White noise circuit used to test the circuit against noise which ranged from -8 V to +8 V.

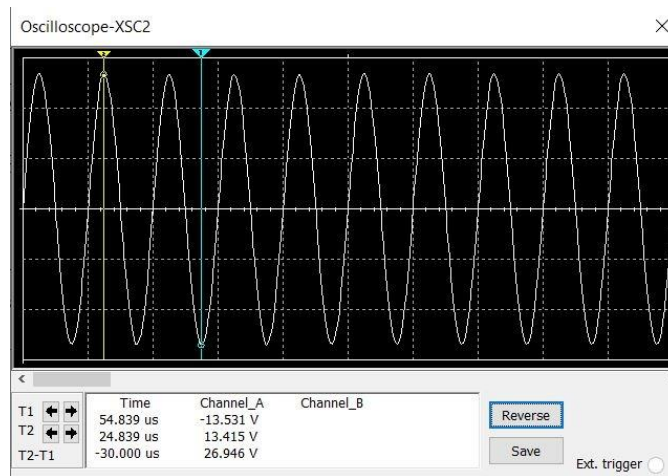


Figure 7. Waveform of input circuit

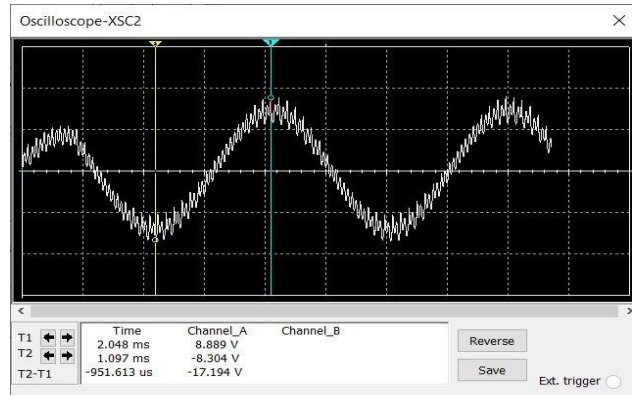


Figure 8 Waveform of input circuit with white noise added

The output of the input AC circuit or the White noise circuit is then fed to the band pass filter circuit to be filtered. The output of band pass filter is then inserted into the operation amplifier circuit, the output after the two circuits shown in Figure 9.

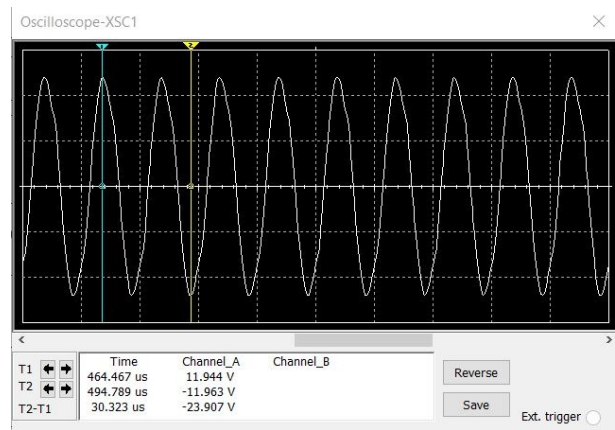


Figure 9 Waveform after band pass filter and operational amplifier circuit

Lastly, after the signal went through the band pass filter and operational amplifier, the signal must be converted to a digital value. Analog-to-digital conversion is an electronic process in which a continuously variable (analog) signal is changed, without altering its essential content, into a multi-level (digital) signal. In EIT system, the final output must be represented in digital value to get the image required to be finally diagnosed, Figure 10 shows the analog-to-digital conversion result (0 - 5 V).



Figure 10 Output of analog-to-digital

## 5. Discussion

The application of EIT treatments in lung related diseases and lung imaging are gaining tremendous attention, including the mechanical ventilation of the disordered lungs. In the case of mechanical ventilation, pressure adjustment is required for the collapsed parts to the mechanical ventilator. During this process, it is necessary to be careful to adjust the pressure properly so that acute lung injury can be prevented over the distending parts of the lungs. Therefore, the control and monitoring of the actual amount of air volume and its distribution should always be observed in real time with proper consideration and precautions during the mechanical ventilation process [31, 32]. Even though EIT systems and their application demonstrate potential promises in monitoring and imaging of the lung functions, their clinical applications are not gaining that much of attention in the professional health care system [33]. One of the most significant reasons of this drawback of the EIT systems is absence of an integrated approach in the EIT based systems that results in the relatively poor resolution in the lung imaging and hardship in obtaining the reliable and related data for an accurate clinical observation.

From the simulation work which integrates several circuit and sub circuit parts, is evident that a signal conditioning circuit can control the EIT system and send accurate signals to the electrodes. The proposed EIT system can be conveniently built with a relatively affordable price, unlike other tomography systems that not only require complex signal conditioning circuits but also stand in need of a high manufacturing price.

The developed 16 channel EIT system could produce functional images of the lungs in a real time integrated approach which is useful in determining the actual air volume supplied to the lungs. The absolute change in the aeration level in the lungs is usually evaluated from the arithmetic difference of two different Positive end-expiratory pressure (PEEP) levels. The difference between the two PEEP levels is also known as end-expiratory lung volume (EELV) [34, 35]. The signal generation and conditioning circuit is critical in this evaluation because it is the main part that supplies the current for reading and presents the real-time screen view. One recent study introduced the lungs collapse models to monitor and observe the image-based functionalities of lungs compliance and over distension collapse. Therefore, with the help of the collapse models, the functional images integrated with the images of time delay techniques could potentially locally determine the collapsed and distended sections or parts of the lungs during the ventilation process. Diagnostic parameters of CoV, A/P ratio, GI, and CV provided useful feedback information during the PEEP titration to recruit collapsed parts of the lungs [34–36]. However, EIT devices could also be used to measure the microscopic phenomena within the respiratory systems induced by the microscopic changes within the airway which shows the importance of a perfectly designed circuit to accommodate and provide accurate measurements. Thus, careful consideration and proper measures should be taken to observe and understand the mechanics of the respiratory systems using the EIT devices. The further development of the EIT devices, both in hardware and software, could enhance the spatial resolution and scanning rates to higher numbers [37–40]. The developed 16 channel EIT system in this study could not only be useful for observation and monitoring the real-time lung imaging, but also in shading an insight into the understanding of circuitry importance and various aspects of clinical and experimental science.

## 6. Conclusion

The simulated circuit demonstrated an approach to design EIT signal conditioning. It is the basis for allowing EIT to visualize the monotonically varying conductivity distribution during inhalation and exhalation in real practice. It assumes that lung conductivity monotonically decreases during inhalation (due to the air flowing into the lungs) and monotonically increases during exhalation (due to the air leaving the lungs). The periodicity of lung ventilation is used to extract its associated current-voltage data; all voltage differences between electrodes increase during inhalation and decrease during exhalation in terms of matrix definiteness regardless of the injection currents. The signal waveform responding to each signal processing stage shows a responding pattern. The output waveform will contribute to the software image reconstruction work to generate tomogram images in practice. EIT unique advantage lies in its capability for continuous monitoring at the bedside. Given the drawbacks of EIT (e.g., technical difficulties of the ill-posed related to EIT data being insufficient to probe local conductivity changes), it is needed to focus on a robust circuit designing method to allow this technique to provide indispensable information in clinical medicine.

## Acknowledgment

Authors acknowledge the Ministry of Higher Education (MOHE) for funding under the Fundamental Research Grant Scheme (FRGS) number: FRGS/1/2021/TK0/UTM/02/66 and UTM Encouragement Research grant (UTMER) Q.J130000.3851.20J51.

## Conflict of Interest

The authors declare no conflict of interest.

## References

- [1] W. R. B. Lionheart, EIT reconstruction algorithms: Pitfalls, challenges and recent developments, *Physiological Measurement*, 2004, 25(1):125–142. <https://doi.org/10.1088/0967-3334/25/1/021>.
- [2] W. Q. Yang and L. Peng, Image reconstruction algorithms for electrical capacitance tomography, *Measurement Science Technology*, 2002, 14(1):R1–R13. <https://dx.doi.org/10.1088/0957-0233/14/1/201>.
- [3] B. H. Brown, Electrical impedance tomography (EIT): A review, *Journal of Medical English Technology*, 2003, 27(3):97–108. <https://doi.org/10.1080/0309190021000059687>.
- [4] L. Borcea, Electrical impedance tomography, *Inverse Problems*, 2002, 18(6):R99–R136. <https://dx.doi.org/10.1088/0266-5611/18/6/201>.
- [5] R. Murthy, Y.-H. Lin, K. Shin and J. L. Mueller, A direct reconstruction algorithm for the anisotropic inverse conductivity problem based on Calderón's method in the plane, *Inverse Problems*, 2020, 36(12). <https://doi.org/10.1088/0266-5611/36/12/012>.
- [6] S. Sun, L. Xu, Z. Cao, J. Sun and W. Tian, Adaptive selection of truncation radius in Calderón's method for direct image reconstruction in electrical capacitance tomography, *Sensors (Basel)*, 2019, 19(9). <https://doi.org/10.3390/s19092014>.
- [7] P. J. Vauhkonen, M. Vauhkonen, T. Savolainen and J. P. Kaipio, Three-dimensional electrical impedance tomography based on the complete electrode model, *IEEE Transactions on Biomedical Engineering*, 1999, 46(9):1150–1160. <https://doi.org/10.1109/10.784147>.
- [8] B. Schullcke, B. Gong, S. Krueger-Ziolek, M. Tawhai, A. Adler, U. Mueller-Lisse and K. Moeller, Lobe based image reconstruction in electrical impedance tomography, *Medical Physics*, 2017, 44(2):426–436. <https://doi.org/10.1002/mp.12038>.
- [9] J. Padilha Leitzke and H. Zangl, A review on electrical impedance tomography spectroscopy, *Sensors (Basel)*, 2020, 20(18). <https://doi.org/10.3390/s20185160>.
- [10] H. Griffiths and A. Ahmed, A dual-frequency applied potential tomography technique: Computer simulations, *Clinical Physics Physiological Measurement*, 1987, 8(Suppl A):103–107. <https://doi.org/10.1088/0143-0815/8/4a/014>.
- [11] E. Barsoukov and J. Ross Macdonald, *Impedance spectroscopy: Theory, Experiment, and Applications*, 2nd ed., New Jersey: John Wiley & Sons, 2005.
- [12] J. Leitzke and H. Zangl, A review on electrical impedance tomography spectroscopy, *Sensors (Basel)*, 2020, 20(18):5160. <https://doi.org/10.3390/s20185160>.
- [13] M. Neumayer, H. Zangl, D. Watzenig and A. Fuchs, Current reconstruction algorithms in electrical capacitance tomography, in: S. C. Mukhopadhyay, A. Lay-Ekuakille and A. Fuchs, *New Developments and Applications in Sensing Technology*, Springer Berlin Heidelberg: Berlin, 2011, 65–106. [http://dx.doi.org/10.1007/978-3-642-17943-3\\_4](http://dx.doi.org/10.1007/978-3-642-17943-3_4).
- [14] G. Singh, S. Anand, B. Lall, A. Srivastava and V. Singh, Low-cost multifrequency electrical impedance-based system (MFEIBS) for clinical imaging: Design and performance evaluation., *Journal of Medical Engineering Technology*, 2018, 42(4):274–289. <http://dx.doi.org/10.1080/03091902.2018.1478008>.
- [15] H. Wu, W. Zhou, Y. Yang, J. Jia and P. Bagnaninchi, Exploring the potential of electrical impedance tomography for tissue engineering applications, *Mater. (Basel, Switzerland)*, 2018, 11(6). <http://dx.doi.org/10.3390/ma11060930>.
- [16] S. Khan, P. Manwaring, A. Borsic and R. Halter, FPGA-based voltage and current dual drive system for high frame rate electrical impedance tomography, *IEEE Transaction on Medical Imaging*, 2015, 34(4):888–901. <https://doi.org/10.1109/tmi.2014.2367315>.
- [17] Y. Yang and J. Jia, A multi-frequency electrical impedance tomography system for real-time 2D and 3D imaging., *Review of Scientific Instruments*, 2017, 88(8):85110. <http://dx.doi.org/10.1063/1.4999359>.
- [18] M. Gehre, T. Kluth, C. Sebu and P. Maass, Sparse 3D reconstructions in electrical impedance tomography using real data, *Inverse Problems in Science and Engineering*, 2014, 22(1):31–44. <https://doi.org/10.1080/17415977.2013.827183>.
- [19] A. McEwan, A. Romsauerova, R. Yerworth, L. Horesh, R. Bayford and D. Holder, Design and calibration of a compact multi-frequency EIT system for acute stroke imaging, *Physiological Measurement*, 2006, 27(5): S199–210. <http://dx.doi.org/10.1088/0967-3334/27/5/S17>.
- [20] R. J. Halter, A. Hartov and K. D. Paulsen, A broadband high-frequency electrical impedance tomography

- system for breast imaging., IEEE Transactions on Biomedical Engineering, 2008, 55(2):650–659. <http://dx.doi.org/10.1109/TBME.2007.903516>.
- [21] J. Padilha Leitzke and H. Zangl, Low-power electrical impedance tomography spectroscopy, International Journal for Computation and Mathematics Electrical and Electronic Engineering, 2019, 38(5):1480–1492. <https://doi.org/10.1108/COMPEL-12-2018-0530>.
- [22] A. Romsauerova, A. McEwan, L. Horesh, R. Yerworth, R. H. Bayford and D. S. Holder, Multi-frequency electrical impedance tomography (EIT) of the adult human head: Initial findings in brain tumours, arteriovenous malformations and chronic stroke, development of an analysis method and calibration, Physiological Measurement, 2006, 27(5):S147–S161. <https://doi.org/10.1088/0967-3334/27/5/s13>.
- [23] H. Ammari, L. Giovangigli, L. H. Nguyen and J.-K. Seo, Admittivity imaging from multi-frequency micro-electrical impedance tomography, Journal of Mathematical Analysis and Applications, 2017, 449(2):1601–1618. <https://doi.org/10.1016/j.jmaa.2017.01.004>.
- [24] M. R. Baidillah, A. S. Iman, Y. Sun and M. Takei, Electrical impedance spectro-tomography based on dielectric relaxation model, IEEE Sensors Journal, 2017, 17(24):8251–8262. <https://doi.org/10.1109/JSEN.2017.2710146>.
- [25] Z. Xu, J. Yao, Z. Wang, Y. Liu, H. Wang, B. Chen and H. Wu, Development of a portable electrical impedance tomography system for biomedical applications, IEEE Sensors Journal, 2018, 18(19):8117–8124. <https://doi.org/10.1109/JSEN.2018.2864539>.
- [26] C. Tan, S. Liu, J. Jia and F. Dong, A wideband electrical impedance tomography system based on sensitive bioimpedance spectrum bandwidth, IEEE Transactions on Instrumentation and Measurement, 2020, 69(1):144–154. <https://doi.org/10.1109/TIM.2019.2895929>.
- [27] T. I. Oh, E. J. Woo and D. Holder, Multi-frequency EIT system with radially symmetric architecture: KHU Mark, Physiological Measurement, 2007, 28(7):S183–S96. <https://dx.doi.org/10.1088/0967-3334/28/7/S14>.
- [28] S. J. Hamilton and J. L. Mueller, Direct EIT reconstructions of complex admittivities on a chest-shaped domain in 2-D, IEEE Transactions Medical Imaging, 2013, 32(4):757–769. <https://doi.org/10.1109/tmi.2012.2237389>.
- [29] E. J. Woo and J. K. Seo, Magnetic resonance electrical impedance tomography (MREIT) for high-resolution conductivity imaging, Physiological Measurement, 2008, 29(10):R1–R26. <https://dx.doi.org/10.1088/0967-3334/29/10/R01>.
- [30] S. J. Hamilton, J. L. Mueller and M. Alsaker, Incorporating a spatial prior into nonlinear D-Bar EIT imaging for complex admittivities, IEEE Transactions on Medical Imaging, 2017, 36(2):457–466. <https://doi.org/10.1109/tmi.2016.2613511>.
- [31] M. C. Bachmann, C. Morais, G. Buggedo, A. Bruhn, A. Morales, J. B. Borges, E. Costa and J. Retamal, Electrical impedance tomography in acute respiratory distress syndrome, Critical Care, 2018, 22(1):263. <https://doi.org/10.1186/s13054-018-2195-6>.
- [32] D. Liu, D. Gu, D. Smyl, J. Deng, and J. Du, shape reconstruction using boolean operations in electrical impedance tomography, IEEE Transactions on Medical Imaging, 2020, 39(9):2954–2964. <http://dx.doi.org/10.1109/TMI.2020.2983055>.
- [33] Z. Li, J. Zhang, D. Liu and J. Du, CT image-guided electrical impedance tomography for medical imaging, IEEE Transactions on Medical Imaging, 2020, 39(6):1822–1832. <https://doi.org/10.1109/TMI.2019.2958670>.
- [34] D. Liu, D. Smyl, D. Gu and J. Du, Shape-driven difference electrical impedance tomography, IEEE Transactions on Medical Imaging, 2020, 39(12):3801–3812. <http://dx.doi.org/10.1109/TMI.2020.3004806>.
- [35] B. Gong, S. Krueger-Ziolek, K. Moeller, B. Schullecke and Z. Zhao, Electrical impedance tomography: Functional lung imaging on its way to clinical practice?, Expert Review of Respiratory Medicine, 2015, 9(6):721–737. <http://dx.doi.org/10.1586/17476348.2015.1103650>.
- [36] L. Zhou, B. Harrach and J. K. Seo, Monotonicity-based electrical impedance tomography for lung imaging, Inverse Problems, 2018, 34(4):45005. <https://dx.doi.org/10.1088/1361-6420/aaaf84>
- [37] C. Kok Seong, J. Puspanathan, R. Abdul Rahim, G. Chiew Loon, Y. Shaan-Li Susiapan, F. A. Phang and M. H. Fazalul Rahiman, Hardware development of electrical capacitance tomography (ECT) system with capacitance sensor for liquid measurements, Jurnal Teknologi, 2015, 73(6). <https://doi.org/10.11113/jt.v73.4399>.
- [38] M. H. Fazalul Rahiman, R. Abdul Rahim, H. Abdul Rahim, Z. Zakaria and J. Puspanathan, A study on forward and inverse problems for an ultrasonic tomography, Jurnal Teknologi, 2014, 70(3). <https://doi.org/10.11113/jt.v70.3473>.
- [39] S. L. Utom, E. J. Mohamad, R. Abdul Rahim, N. Yeop, H. L. Mohamad Ameran, H. Abdul Kadir, S. Z. Mohd Muji and J. Puspanathan, Non-destructive oil palm fresh fruit bunch (FFB) grading technique using optical sensor, International Journal of Integrated Engineering, 2018, 10(1):35–39. <https://doi.org/10.30880/ijie.2018.10.01.006>.

- [40] F. R. Mohd Yunus, N. A. Noor Azlan, N. M. Nor Ayob, J. Pusppanathan, M. F. Jumaah, C. L Goh, R. Abdul Rahim, A. Ahmad, Y. M. Yunus and H. Abdul Rahim, Simulation study of bubble detection using dual-mode electrical resistance and ultrasonic transmission tomography for two-phase liquid and gas. *Sensors and Transducers*, 2013, 150(3):97–105. <https://doi.org/10.1016/j.powtec.2014.02.001>.